Biophysical Journal, Volume 97

Supporting Material

Flickering Analysis of Erythrocyte Mechanical Properties: Dependence on Oxygenation Level, Cell Shape and Hydration Level

Young-Zoon Yoon, Ha Hong, Aidan Brown, Dong Chung Kim, Dae Joon Kang, Virgilio L. Lew, and Pietro Cicuta

Protocol to control hydration state of RBC

The normal K^+ concentration in human RBCs is about 130-140 mM and the membrane potential is about -10 mV. K^+-permeabilized RBCs will thus gain or lose KCl and water depending on whether they are suspended in isotonic media containing more or less than 100 mM K^+, the external K^+ concentration at electrochemical equilibrium with normal intracellular K^+. Transient K^+ permeabilization was obtained by a brief Ca^{2+} load which activated the endogenous Ca^{2+}-sensitive K^+ channels of the RBC membrane (Gardos channels, IK1, KCNN4). The Ca^{2+} load, in turn, was induced by exposure of the RBCs to the divalent cation ionophore A23187. After allowing time for K^+ equilibration, Ca^{2+} was extracted from the cells by adding a large excess of EGTA over calcium in the medium, thus switching off the Gardos channels. The ionophore was then washed away with the use of bovine serum albumin and the normal low original Ca^{2+} permeability of the RBCs was restored. The rate of K^+ equilibration is usually limited by the relatively low anion permeability. Partial replacement of Cl^- by the much more permeable anion SCN^- allowed rapid equilibration thus preventing the side-effects of prolonged exposure to elevated intracellular Ca^{2+}.

The experimental protocol was implemented as follows. About 10 ml of blood were drawn into heparinized syringes. Fresh RBCs were washed twice by centrifugation and resuspension in over 10 volumes of wash medium A containing (in mM) NaCl, 140, KCl, 3, Na-HEPES (pH 7.5), 10, and $MgCl_2$, 0.15, with 0.1 mM Na-EGTA, and twice more with medium A. The buffy coat was removed after each wash. After the last wash, four different cells suspensions (labeled as: control, 3K, 50K and 120K) were prepared, all at 5% haematocrit and all in isotonic medium B (in mM: NaSCN, 10, Na-HEPES (pH 7.5), 10, $MgCl_2$, 0.15, $CaCl_2$, 0.1, and inosine, 5, plus the following KCl/NaCl concentrations (in mM): 3/140 for control and 3K, 50/93 for 50K, and 120/23 for 120K). The suspensions were incubated at 37^oC under magnetic stirring. After about 5 minutes, to allow for temperature equilibration, the ionophore A23187 was added ($t = 0$) to give a final concentration of 10μM in each suspension (except in the control group A) and the incubation was continued for a further 10 minutes to allow for full K^+ equilibration. At $t = 10$ minutes, Na-EGTA (1 mM) was added to each suspension to extract Ca^{2+} from the cells and deactivate the Gardos channels. About 5 minutes later, each suspension was transferred into centrifuge tubes containing 10 volumes of ice-cold medium A supplemented with 0.1 mM EGTA and 1% defatted bovine serum albumin, to initiate the extraction of the ionophore A23187. The cells were washed thrice by centrifugation and resuspension

in the same medium at a volume-cell ratio of about 100:1, and finally suspended at 5% haematocrit in A for volume analysis by osmotic fragility distribution, as detailed before (1). Small aliquots from each group were suspended in medium A supplemented with 0.1 mM Na-EGTA and 0.1% BSA for fluctuation and Raman analysis. Figure SM1 shows the osmotic fragility curves for the four samples described above. For the purpose of comparing with other in-vitro and intra-cell experiments, the haemoglobin concentrations corresponding to each of the conditions tested were estimated from model simulations using the Lew-Bookchin red cell model (2), and are expressed in units of g/dl, equivalent to the commonly used mean corpuscular haemoglobin concentration in the medical literature. The haemoglobin concentrations studied are as follows: 24g/dl (sample 120K), 34g/dl (control sample), 45g/dl (sample 50K), 57g/dl (sample 3K).

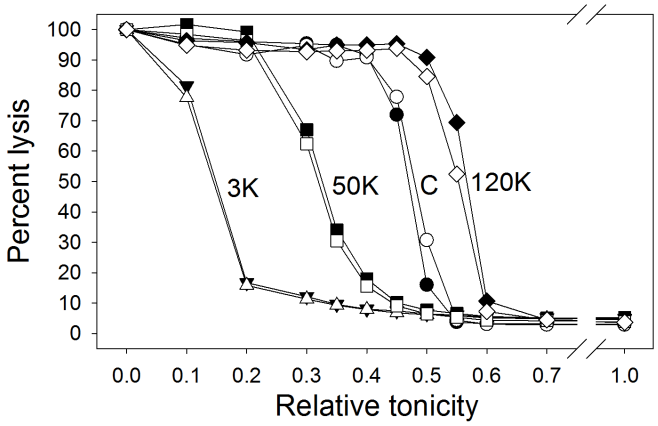

Supplementary Figure SM1: Osmotic fragility curves of RBCs equilibrated at the indicated K^+ concentrations. The control curves (C) of untreated RBCs show the normal error function distribution which characterizes the osmotic fragility pattern of normal RBCs (3), with 50% lysis at about 0.5 relative tonicity (relative to physiological osmolalities of about 290 mOsmolal). Shifts to the right indicate overhydration whereas shifts to the left indicate dehydration. It can be seen that the cells equilibrated in 3 and 50 mM external K^+ show extreme and moderate dehydration, respectively, whereas those equilibrated in 120 mM K^+ are moderately overhydrated relative to untreated controls. Clear and filled symbols correspond to duplicate curves for each condition.

Contour detection

The contour of the cell membrane was detected by an algorithm developed in house and coded as a c++ module called within Matlab. The essential steps are outlined in Fig.1 of the manuscript, and described here in detail:

- a) the center of the cell is determined for each frame;
- b) the image is resampled along equally spaced radial lines diverging from the cell center determined at step (a), and each resampled line profile is normalized to make a set of profiles within inner and outer bounds, as shown in Fig.1(b) and (c);
- c) a correlation kernel is created: the profiles of step (b) from the first frame are aligned with each other by matching their maximum gradient points, and these are averaged together to create a kernel for correlation;
- d) using the correlation kernel of step (c), a correlation value is calculated for each line profile at each radial position, resulting in a correlation array such as Fig.1(d) for each frame;
- e) the correlation profiles of step (d) show a well defined peak at the cell boundary, and this is fit to a quadratic function to extract the boundary position at sub-pixel resolution, as shown by the dotted line in Fig.1(d).

Compared to previous analysis of contour position (4, 6), our use of a correlation kernel gives a slight improvement on contour position detection over fitting a linear profile to the contour derivative. The position of each point is known to within an error δr of a few nm. However the most significant benefit of fitting several hundred points on the contour is that the position information from every one of these points (which are determined independently of each other) is used to determine the amplitude of modes. The error on the mode amplitude $\delta h_n$is thus reduced compared to the error on individual contour points: following this argument, the error on mode n is roughly equal to $\delta x\sqrt(n/360)$. At the highest mode that we plot in Figure 2 (manuscript), $n = 20$, the error on the mode amplitude is thus $\sim \delta x/4$, which is below 1nm. At higher modes, the signal decreases and the error on the mode amplitude increases, so the spectrum levels off (data not shown in Fig. 2).

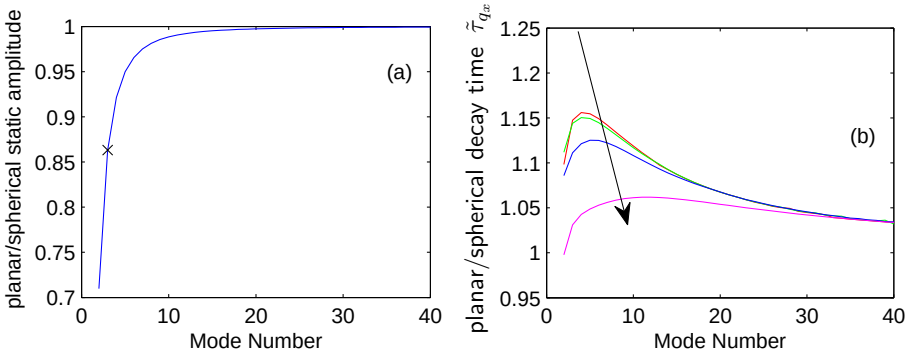

Supplementary Figure SM2: Modeled data showing that the planar continuous membrane approximation to a closed membrane is appropriate above mode $n = 3$. Membrane parameters are $R = 4\,\mu$m; $\sigma = 5 \times 10^{-7}\,\mathrm{Nm}^{-1}$; $\kappa = 25 \times 10^{-20}\,$J; T=300 K, which are representative of the conditions in the RBC experiment. (a) Ratio of the mean square amplitude of fluctuations as a function of mode number, calculated for the planar approximation detailed in the text, and for discrete spherical modes as described in (4). An (×) marks mode $n = 3$. (b) Ratio of the decay times of equatorial fluctuation modes as a function of mode number, calculated for the planar approximation detailed in the text, and for discrete spherical modes as described in (5). Arrow indicates increasing RBC cytoplasmic viscosities $\eta_{int} = (1, 2.5, 10, 100) \times 10^{-3}\,$Pa s; and water is taken to have $\eta_{out} = 10^{-3}\,$Pa s.

Planar membranes with tension and bending

In this section the classical derivation of the membrane fluctuation spectrum is reproduced, for the case of a planar continuous membrane with tension and bending modulus. This is extended to consider further contributions in the manuscript.

The free energy functional to consider small amplitude membrane fluctuations is (7):

$$F = \int_A d\vec{x} \left[\frac{1}{2}\sigma(\nabla h)^2 + \frac{1}{2}\kappa(\nabla^2 h)^2 \right], \tag{S1}$$

where $A = L \times L$ is the area of the membrane. The displacement $h(\vec{x})$ can

be expressed in terms of its Fourier modes $h_{\vec{q}}$:

$$h(\vec{x}) = \frac{A}{(2\pi)^2} \int d\vec{q}\, h_{\vec{q}}\, e^{i\vec{q}\cdot\vec{x}}, \tag{S2}$$

where

$$h_{\vec{q}} = \frac{1}{A} \int d\vec{x}\, h(\vec{x})\, e^{-i\vec{q}\cdot\vec{x}}, \tag{S3}$$

and from energy equipartition it is possible to relate the mean square amplitude of each mode to the membrane bending modulus (κ) and tension (σ):

$$\left\langle h_q^2 \right\rangle = \frac{k_B T}{A} \frac{1}{\sigma q^2 + \kappa q^4}, \tag{S4}$$

where $q^2 = q_x^2 + q_y^2$, k_B is the Boltzmann constant, and T is the absolute temperature. The power spectrum of Eq. S4 is correct in the limit of small deformations of an infinitely large membrane. There are also equivalent formulations in terms of the discrete modes of a closed vesicle (or cell), but the two are well known to be equivalent in practice for all but the lowest deformation modes. These equations S1–S4 have been used successfully and extensively in the study of membrane fluctuations (4, 8, 9).

Comparison of planar and spherical membranes

Figure SM2 compares the planar and spherical models for static amplitude and dynamical behavior as a function of mode numbers. Panel (a) shows that above mode $n = 3$ the planar and geometrical models are within 15% of each other. Panel (b) similarly shows that the difference between the two models is less than 15% over the whole possible range of cytoplasmic viscosities.

Analysis of the effect of equatorial projection on contour mode dynamics

Because of the various q dependencies in Eq.7 (manuscript), observing the dependence of the timescale $\tau_{\vec{q}}$ on the mode number informs on possible alternative behavior, as summarized in Figure SM3(a). On the other hand the observed $q-$dependence of model dynamics renders information on membrane properties.

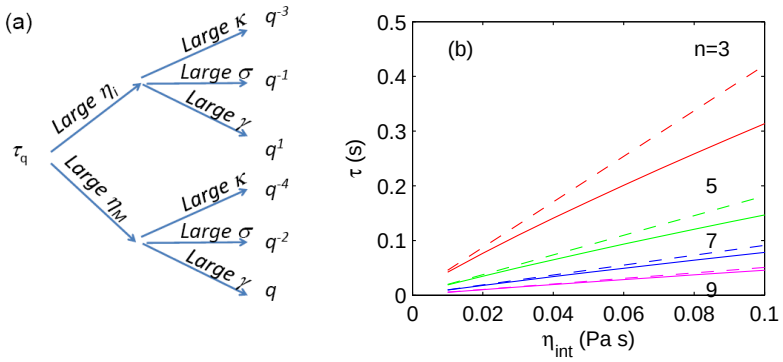

Supplementary Figure SM3: (a) Schematic showing the six possible limiting conditions on the behaviour of τ_q as a function of q, depending on the dominant characteristics of the membrane. (b) Panel showing the effect of equatorial contour projection on the decay times of fluctuation modes. Calculated values of planar modes $\tau_{\vec{q}}$ (dashed line) and projected modes $\tilde{\tau}_{q_x}$ (solid line) are shown as a function of the internal viscosity of the cell η_{int}, for modes numbered 3,5,7,9. Parameters are the same as in Figure SM2. The calculation shows that $\tau_{\vec{q}}$ is around 25% larger than $\tilde{\tau}_{q_x}$, and this correction is roughly mode- and viscosity-independent. In other words, it is possible and simple to take into account the effect of projection of q_y-modes onto the equatorial contour, as in Eq. 8 (manuscript), when interpreting the relaxation timescales of contour modes.

Numerical integration confirms that the correlation function $\tilde{C}_{q_x}(t)$ defined in Eq.8 (manuscript) is also a simple exponential decay, like $C_{\vec{q}}(t)$. This is shown in Fig.3(b) of the manuscript, where the contour relaxations are interpolated by an exponential relaxation. We label this decay timescale $\tilde{\tau}_{q_x}$. The modes for which we can follow the time decay accurately are those from 5 to 9. Higher modes decay over timescales that are short, and comparable with our frame rate, and hence their relaxation timescale cannot be determined accurately in our current experiments. Figure SM3(b) compares the calculated values of the exponential relaxation timescale for $C_{\vec{q}}(t)$ and $\tilde{C}_{q_x}(t)$, as a function of the cytoplasmic viscosity, for a few mode numbers. It can be seen that the projection of the q_y modes onto the equator leads to a decrease in the decay time, i.e. corresponds to a faster observed decay. This effect is roughly constant over the range of modes and viscosities that can be observed, with the experimentally observed $\tilde{\tau}_{q_x} \simeq 0.8\,\tau_{\vec{q}}$.

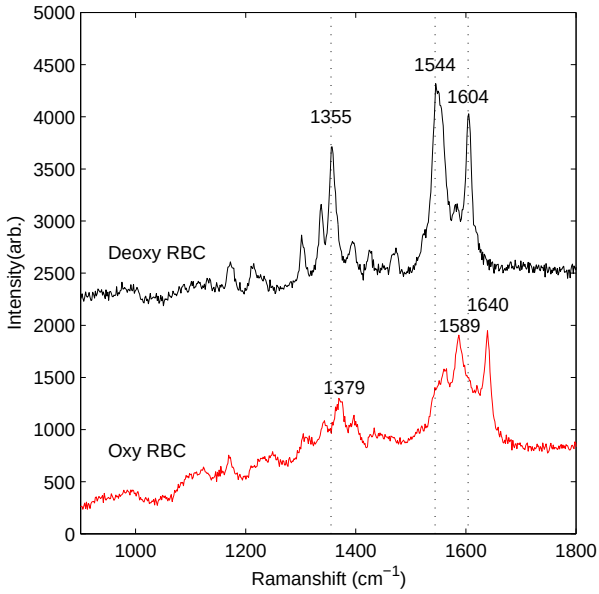

Supplementary Figure SM4: Raman Spectra of a single RBC in both the oxygenated and deoxygenated states recorded after the addition of $Na_2S_2O_4$. All spectra are recorded in PBS using the 514 nm HeNe laser. For each spectrum three intermittent scans are accumulated with a 10 s laser exposure time. The dashed lines in the spectra indicate bands that appear clearly following deoxygenation.

Raman Spectra

The consensus view is that the out of plane translocation of the haem Fe from the porphyrin plane triggers the R (relaxed with a higher oxygen concentration) to T (tense with lower oxygen concentration) transition in haemoglobin (Hb) (10). The Raman spectrum detects this translocation and thus reports the oxygenation state of haemoglobin. The 1650–1500 cm^{-1} peak in all spectra consists mainly of porphyrin in-plane vibrational modes that are sensitive to porphyrin distortion. The disappearance of the 1640 cm^{-1} peak is indicative of porphyrin doming, which is in good agreement with other Raman studies (10, 11). The 1400–1300 cm^{-1} peak in the Raman spectra is considered as the oxidation and spin state of the central metal atom within the porphyrin macrocycle (12). Here the 1379 cm^{-1} is dominant for the oxygenated form of hemoglobin and the 1355 cm^{-1} is typical of the deoxygenated form.

References

1. Tiffert, T., V. L. Lew, H. Ginsburg, M. Krugliak, L. Croisille, and N. Mohandas, 2005. The hydration state of human red blood cells and their susceptibility to invasion by *Plasmodium falciparum*. *Blood* 105:4853.

2. Lew, V. L., and R. M. Bookchin, 1986. Volume pH and ion content regulation in human red cells: analysis of transient behaviour using an integrated mathematical model. *Journal of Membrane Biology* 92:57–74.

3. Raftos, J. E., R. M. Bookchin, and V. L. Lew, 1996. Distribution of chloride permeabilities in normal human red cells. *J. Physiol.* 491:773–777.

4. Pecreaux, J., H. G. Dobereiner, J. Prost, J. F. Joanny, and P. Bassereau, 2007. Refined contour analysis of giant unilamellar vesicles. *Eur. Phys. J. E* 13:277.

5. Peterson, M. A., 1992. Linear response of the human erythocyte to mechanical stress. *Phys. Rev. A* 45:4116.

6. Strey, H., M. A. Peterson, and E. Sackmann, 1995. Measurement of Erythrocyte Membrane Elasticity by Flicker Eigenmode Decomposition. *Biophysical J.* 69:478–488.

7. Helfrich, W., and R. M. Servuss, 1984. Undulations, steric interaction and cohesion of fluid membranes. *Nuovo Cimento D* 3:137.

8. Brochard, F., and J. F. Lennon, 1975. Frequency spectrum of the flicker phenomenon in erythrocytes. *J. Phys. France* 36:1035–1047.

9. Safran, S. A., 1994. Statistical theomodynamics of surfaces, interfaces, and membranes. Addison-Wesley, Reading, Massachusetts.

10. Strekas, T. C., and T. G. Spiro, 1972. Resonance Raman Spectra of Hemoglobin and Cytochrome c: Inverse Polarization and Vibronic Scattering. *Proc. Natl. Acad. Sci.* 69:2622–2626.

11. Wood, B. R., B. Tait, and D. McNaughton, 2001. Micro-Raman characterization of the R to T state within a single living erythrocyte. *Biochim. Biophys. Acta* 1539:58.

12. Carey, P., 1982. Biochemical Applications of Raman and Resonance Raman Spectroscopies. Academic Press, London (U.K.).